Immobilization of Soluble Protein Complexes in MAS solid-state NMR: Sedimentation versus Viscosity

Riddhiman Sarkar,[1,2] Andi Mainz,[1,2,3] Baptiste Busi,[1,2,4] Emeline Barbet-Massin,[1,2] Maximilian Kranz,[4] Thomas Hofmann,[4] and Bernd Reif[1,2,*]

March 10, 2016

[1] Munich Center for Integrated Protein Science (CIPSM) at Department of Chemie, Technische Universität München (TUM), Lichtenbergstr. 4, D-85747 Garching, Germany

[2] Helmholtz-Zentrum München, Deutsches Forschungszentrum für Gesundheit und Umwelt (HMGU), Ingolstädter Landstr. 1, D-85764 Neuherberg, Germany

[3] Technische Universität Berlin, Fakultät II Mathematik und Naturwissenschaften, Institut für Chemie / OC / Biologische Chemie, Müller-Breslau-Straße 10, 10623 Berlin

[4] Chair of Food Chemistry and Molecular Sensory Science, Technische Universitaẗ München, Lise-Meitner-Strasse 34, 85354 Freising, Germany

For submission to: *Solid-state NMR* (Trends Article)

*Correspondence should be addressed to reif@tum.de

ABSTRACT

In recent years, MAS solid-state NMR has emerged as a technique for the investigation of soluble protein complexes. It was found that high molecular weight complexes do not need to be crystallized in order to obtain an immobilized sample for solid-state NMR investigations. Sedimentation induced by sample rotation impairs rotational diffusion of the protein and enables efficient dipolar coupling based cross polarization transfers. In addition, viscosity contributes to the immobilization of the molecules in the sample. Natural Deep Eutectic Solvents (NADES) have very high viscosities, and can replace water in living organisms. We observe a considerable amount of cross polarization transfers for NADES solvents, even though their molecular weight is too low to yield significant sedimentation. We discuss how viscosity and sedimentation both affect the quality of the obtained experimental spectra. The FROSTY/sedNMR approach holds the potential to study large protein complexes, which are otherwise not amenable for a structural characterization using NMR. We show that using this method, backbone assignments of the symmetric proteasome activator complex (1.1 MDa), and high quality correlation spectra of non-symmetric protein complexes such as the prokaryotic ribosome 50S large subunit binding to trigger factor (1.4 MDa) are obtained.

GRAPHICAL ABSTRACT

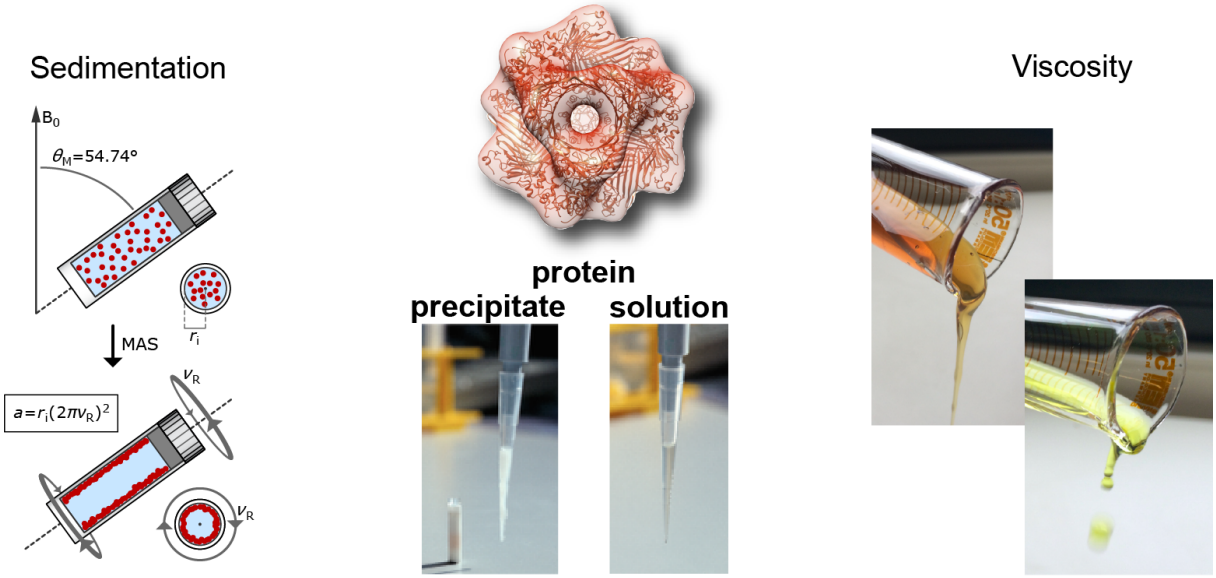

HIGHLIGHTS

- Large protein complexes in solution can be investigated by MAS NMR
- Rotor spinning induces sedimentation to immobilize the sample
- Viscosity contributes to the impairment of rotational diffusion
- Sensitivity increases beyond quantitative sedimentation

INTRODUCTION

In the last years, magic-angle spinning (MAS) solid-state NMR has emerged as a powerful analytical technique to study the structural properties of non-soluble biomolecules, such as amyloid fibrils [1, 2] and membrane proteins [3, 4]. In addition, however, also techniques are needed that allow for characterization of heterogeneous systems in structural biology. In this context, large soluble protein complexes that are too dynamic for crystallographic studies are of particular interest. For example, hetero-complexes formed between misfolding peptides or proteins and molecular chaperones which prevent aggregation are very difficult to study with conventional techniques. These heterogeneous complexes have molecular weights which are in the range of several megadaltons. In traditional solid-state NMR approaches, chaperone and amyloid substrate need to be co-crystallized/co-precipitated to study the interaction. This co-precipitation is often difficult when the chaperone is very soluble, and the amyloid substrate very hydrophobic. The FROSTY/sedNMR approach which is reviewed in this article, presents an alternative to characterize these systems by NMR spectroscopy.

In MAS solid-state NMR, immobilized samples are spun rapidly in a cylindrical rotor, which is inclined at an angle Θ_{MA} of 54.74° relative to the magnetic field of the NMR spectrometer [5]. Line narrowing by MAS is achieved if the rotational/tumbling correlation time of the investigated molecules is much larger than the rotor period. This is obviously the case for an immobilized solid sample. However, this also holds true for a solution of a high molecular weight protein at low temperature and high viscosity [6, 7]. To account for this, we introduced the acronym "FROSTY" (**F**reezing **R**otational diffusion **O**f protein **S**olutions at low **T**emperature and high viscosit**Y**). Bertini et al. have suggested that strong centrifugal forces during MAS lead to reversible protein sedimentation [8] which effectively induces immobilization of the protein. Therefore, the acronym "sedNMR" was coined for these kind of experiments. In fact, the tumbling correlation time of protein complexes such as αB-crystallin that have a molecular weight of ca. 600 kDa amounts to only a few µs in the absence of MAS [9]. It is remarkable that this approach allows to overcome the molecular weight limit imposed by molecular tumbling in classical solution-state NMR. Megadalton protein complexes are now accessible which previously could only be investigated in selectively methyl labeled samples in solution-state NMR [10]. The FROSTY/sedNMR approach allows to circumvent sample preparation issues. Selection of the proper precipitation conditions is not anymore necessary. For ligand binding studies, crystallization with and without ligand can yield different crystal forms that result in differential spectral patterns. This complicates the analysis of chemical shift perturbations. In particular for weakly interacting systems, such as misfolding peptides and proteins binding to molecular chaperones, this approach might be an interesting alternative to crystallization, as the two components are very much different in terms of their solubility and co-precipitates are thus difficult to obtain. In addition, inhomogeneous line broadening due to chemical shift disorders and anisotropic magnetic susceptibility present in solid samples can be minimized by this approach.
One might argue that biological solid-state samples such as fibrils or membrane proteins are always prepared by sedimentation [11]. In that sense, the FROSTY/sedNMR approach is not

novel. The transitions are obviously seamless and the discussion might appear to be semantic. We would like to emphasize here, however, that FROSTY/sedNMR allows to study and access much smaller protein complexes which were so far a domain of classical solution-state NMR.

Figure 1A shows ^{13}C detected cross polarization (CP) buildup curves for a ^{13}C, ^{15}N labeled solution-state sample of the small heat-shock protein αB-crystallin spinning with a MAS rotation frequency of 12 kHz. The MAS frequency dependent ^{13}C CP signal intensity at constant temperature is represented in Figure 1B. Cross polarization builds up within 100 µs indicating an order parameter which is close to 1. The CP signal can only be observed in case the MAS rotation frequency is high enough, suggesting that above a rotation frequency of 8 kHz most of the protein is immobilized at the inner walls of the solid-state NMR rotor.

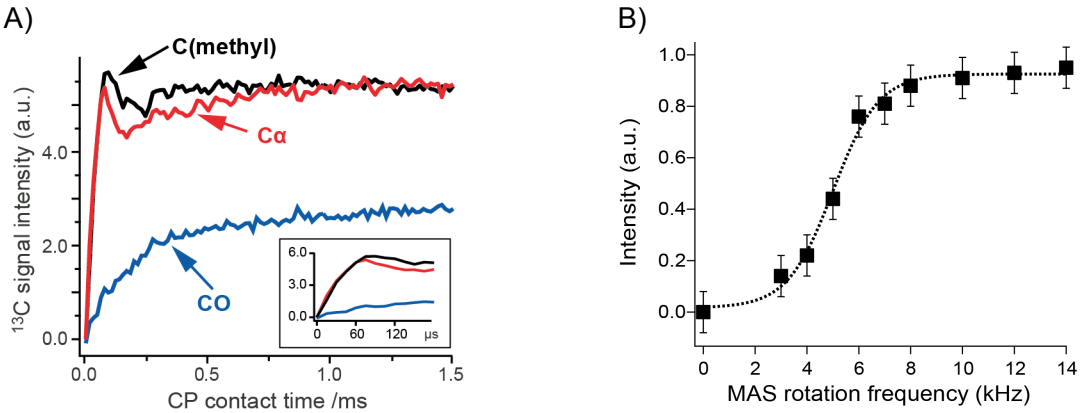

Figure 1. (A) ^{1}H, ^{13}C CP build up curves for carbonyl (blue), Cα (red) and methyl resonances (black) of a 4 mM (monomer) solution of ^{13}C,^{15}N αB-crystallin rotating at a MAS frequency of 10 kHz and at an effective temperature of 10 °C. The inset focusses on the first 180 µs of the cross polarization build up. Reproduced with permission of the American Chemical Society from Mainz et al. [6]. (B) ^{1}H, ^{13}C CP intensities for ^{13}C,^{15}N αB-crystallin as a function of the MAS rotation frequency in a 3.2mm MAS rotor.

Applications

After the first experimental demonstration [6, 8], the FROSTY/SedNMR approach has found wide spread application in the investigation of high-molecular weight biological systems.

The approach was successfully implemented to determine the metal binding sites in the small heat-shock protein (sHSP) αB-crystallin [7]. The human sHSP αB-crystallin (αB) is a 175-residue protein (20 kDa), which assembles into polydisperse and highly dynamic protein complexes of molecular weights ranging between 200–1000 kDa [12, 13]. It is known that elementary Cu(II) binds with picomolar affinity to αB-crystallin [14] and increases the chaperone activity of αB [15]. It was demonstrated that the α-crystallin domain is specifically coordinating one Cu(II) ion involving the amino acids His-83, His-104, His-111 and Asp-109 near the dimer interface. The involvement of Asp-109 has direct implications for dimer stability as this residue forms a salt-bridge with the disease-related Arg-120 of the neighboring monomer. Furthermore, we observe structural reorganization of strands β2-β3

triggered by Cu(II)-binding. This N-terminal region is known to mediate both the intermolecular arrangement in αB oligomers and the binding of client proteins. In the presence of Cu(II), the size and the heterogeneity of αB multimers are increased. We therefore suggested that Cu(II)-binding unblocks potential client binding sites and alters quaternary dynamics of both the dimeric building block as well as the higher-order assemblies of αB.

Solutions of the Alzheimer's disease peptides Aβ40 and Aβ42 have been employed to study oligomer formation [16]. Simultaneous observation of INEPT and CP signal intensities allowed to quantify low and high oligomer Aβ aggregation states. As the oligomerization kinetics are significantly slower in comparison to the sedimentation process, it is followed that the increase in CP NMR signal intensities as a function of time actually reports on the kinetics of oligomerization. A pre-sedimented oligomeric Aβ sample with a specific molecular weight allowed to yield a partial resonance assignment of the Aβ oligomeric state. Ex-situ sedimentation using a commercial preparative ultracentrifuge [11, 17, 18] turned out to be an excellent tool to pack MAS solid-state NMR rotors in general. This tool did not only become indispensable for packing any amyloid fibril and membrane protein sample, but turned out to be also beneficial for Dynamic Nuclear Polarization (DNP) sample preparation. Cryo-protectants such as glycerol are not needed to prevent ice crystal formation. The protein sediment can form a glass with the DNP free radical at the wall of the rotor, whereas the bulk water in the sample forms ice upon freezing in the centre of the rotor [19]. For the 480 kDa 24-mer apoferritin, sedimentation yielded a 20-fold increase in sensitivity compared to DNP with conventional sample preparation.

In case the molecular weight of a phospholipid nanodisc reconstituted membrane protein exceeds the molecular weight limit imposed by solution-state NMR, ex-situ sedimentation in combination with FROSTY/sedNMR provides an alternative way for a structural analysis of the system [20]. Marassi and co-worker have shown that the membrane protein Ail reconstituted in MSP1D1Δh5 nanodiscs [21] yields high-quality $^{13}C,^{13}C$ correlation spectra. Solution-state NMR ^{1}H, ^{15}N TROSY spectra obtained after dilution of the sediment are very similar to the spectra obtained before sedimentation, suggesting that sedimentation does not interfere with the conformational properties of the samples.

FROSTY/sedNMR has further been used to characterize chaperone-amyloid interactions [22]. In αB-crystallin, the monomeric subunit is organized in three regions: the central α-crystallin domain (ACD) comprising residues 60–150, as well as the flanking N-terminal domain (NTD) and C-terminal domain (CTD). The CTD harbors a highly conserved IXI-motif (residues I159, P160 and I161 in αB), which has been reported to interact with adjacent subunits [23-26]. Structural insights into oligomer architecture came from magic-angle spinning (MAS) solid-state NMR spectroscopy employing precipitated full-length αB [23, 27, 28]. In combination with small-angle X-ray scattering (SAXS) and cryo-electron microscopy (cryo-EM), two structural models for 24-mers have been suggested [23, 29]. Although differing in their

details, both 24-mer models propose a tetrahedral symmetric arrangement of four hexameric rings, each consisting of three dimeric subunits. The hexameric sub-structure is stabilized by anchoring the C-terminal IPI-motif to the hydrophobic β4–β8 groove (dimer interface II) of a neighboring protomer [23, 29]. In both models, the dimer consists of structurally different protomers and thus appears asymmetric. In the pseudo-atomic model derived from cryo-EM, the two protomers have been designated as the extended and bent conformers, which differ in the orientation of their NTDs and CTDs with respect to their ACDs (Figure 2). For example, the two CTDs of a dimer reside in different positions: the CTD of the bent conformer (CTD_{bent}) is fairly solvent-exposed (only restricted by its interactions with neighboring β4–β8 grooves), whereas the CTD of the extended conformer (CTD_{ext}) is oriented towards the interior of the complex. A doubling of peaks was only observable due to the favorable resolution of the additional proton dimension in the experiments. Experiments that exclusively rely on heteronuclear detection fail to detect the second set of peaks (Figure 2B). αB-crystallin is an efficient holdase. In case, a substrate such as reduced lysozyme is added to αB-crystallin, lysozyme is not precipitating any longer, but stays soluble in solution (Figure 2C). As a consequence of binding of lysozyme to αB-crystallin, defined chemical shift changes are observed for residues in the hydrophobic β4–β8 groove (Figure 2C, bottom).

To yield high resolution proton spectra in the solid-state, ^{1}H, ^{1}H dipolar couplings can be chemically suppressed by perdeuteration of the sample. If the respective perdeuterated protein is recrystallized from a buffer containing 90% D_2O, ultra-high resolution ^{1}H detected MAS solid-state NMR spectra are obtained at intermediate rotation frequencies (10-20 kHz) [30, 31]. Similarly, high-resolution spectra can be recorded for methyl protons in perdeuterated peptides and proteins by using specifically protonated amino acid precursors [32, 33]. Alternatively, bacteria are grown in a deuterated medium which is doped with defined amounts of H_2O, resulting in stochastic incorporation of protons in all (non-exchangeable) sites [34-37]. Use of protonated amino acids in an otherwise deuterated matrix represents another possibility to achieve high resolution in a direct proton evolution period [38]. At faster spinning (60 kHz), recrystallization of the sample from a buffer containing 100% H2O yields comparably high resolution [39]. In addition to the above mentioned experiments involving soluble protein complexes, the deuteration approach has been applied to amyloid fibrils [40-42] and membrane proteins [4, 43], virus nucleocapsids [44], bacterial secretion needles [45]. Recent developments in MAS probe technology allows now to increase rotation frequencies up to 110 kHz [46-48]. At the same time, the sample volume is reduced to 0.8 µL. The smaller rotor diameter results in a greater acceleration of the protein complexes in solution which facilitates FROSTY / sedNMR applications.

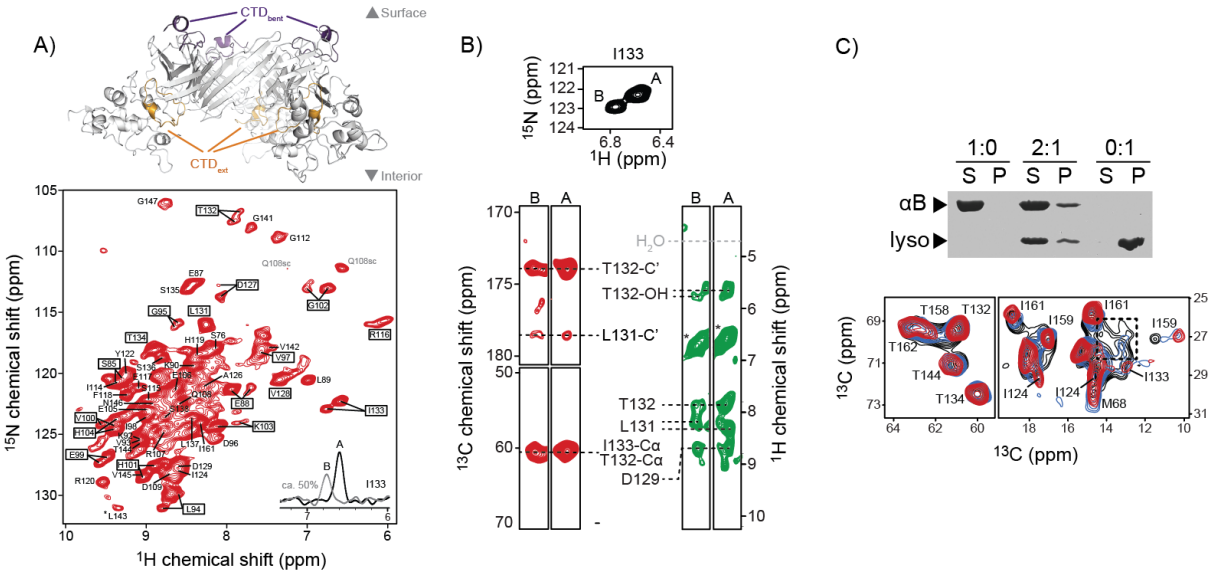

Figure 2. (A) Structural representation of the small heat shock protein αB-crystallin focussing on the hexameric ring formed by three asymmetric dimers (top, PDB: 2YGD). The C-terminus of the extended conformer CTD_{ext} (orange) is involved in interactions with the N-terminal domain NTD_{ext}, whereas CTD_{bent} (purple) is fairly solvent-accessible. ^{1}H,^{15}N correlation spectrum of u-[^{2}H,^{13}C,^{15}N]-αB-crystallin. Exchangeable sites were back-substituted with 20% protons to yield efficient suppression of proton, proton dipolar interactions. Two sets of resonances are observed which are tentatively assigned to the two conformers in the basic dimeric building block. (B) Section of the ^{1}H-^{15}N correlation MAS NMR spectrum of perdeuterated αB (black) showing the two cross-peaks for I133 (A and B). The corresponding 2D strips of the 3D hCXhNH spectra (red) show that the chemical shifts are degenerate in the ^{13}C dimension for both states. The introduction of a ^{1}H dimension allows to resolve the two structural states. A 3D ^{1}H-^{1}H RFDR experiment (2D strips extracted at the same ^{15}N frequency, in green) yield spatial connectivities between the backbone amides of I133-A and -B and the neighboring loop residues (including side-chain hydroxyl groups). The asterisks denote diagonal peaks. (C) SDS-PAGE of samples containing varying molar ratios of αB and lysozyme (Lyso) (top). Threonine (left) and isoleucine spectral region (right) of ^{13}C-^{13}C correlation MAS NMR spectra of αB in the absence (red), in the presence of sub-stoichiometric (blue) and stoichiometric (black) amounts of unlabeled lysozyme unfolded by the addition of TCEP. Upon titration of lysozyme, additional isoleucine signals become observable (dashed box) (bottom). Reproduced with permission of Nature Publishing Group from Mainz et al. [22].

In addition to homo-oligomeric protein complexes, the FROSTY/sedNMR approach is also applicable for protein complexes that lack symmetry [49]. To estimate the expected sensitivity, we performed the following calculation: In the experiments involving the highly symmetric $11S_{14}$-$\alpha_7\beta_7\beta_7\alpha_7$ complex of the 20S proteasome (*Thermoplasma acidophilum*), the (initial) particle concentration amounted to ca. 200 µM [10]. In this case, the sample was directly pipetted into the MAS rotor without the help of an ultracentrifuge packing device. With this sample, we achieved a signal-to-noise ratio on the order of 30-90:1 in an overnight experiment (20% exchangeable protons in an otherwise perdeuterated environment, 3.2 mm rotor, 20 kHz). For a prokaryotic ribosome with a molecular weight on the order of 2.5 MDa (that is lacking the 14-fold symmetry of the 20S proteasome), a (theoretical) maximum concentration in the sediment of 400 µM can be obtained (c_{limit} = ca. 0.7 $\rho_{protein}/M_W$ for tightest packing of spheres). To achieve this concentration, the sample was sedimented ex-situ using an ultracentrifuge. The expected signal-to-noise ratio for this kind of sample would be on the order of 4-13:1 for a 12 h experiment. This sensitivity can be further increased by making use of fast spinning (1.3 mm) rotors. It has been shown that the same proton line width and resolution is obtained for perdeuterated protein samples that are fully proton back-substituted and rotated at 60 kHz (1.3 mm) in comparison to perdeuterated samples that contain only

20% protons at exchangeable sites and which are spun at 20 kHz (3.2 mm) [31, 39]. A factor of 5 in sensitivity is thus obtained due to the increased proton enrichment of the sample. Another factor of 2.5 is obtained due to the increased quality factor of the smaller diameter coil. The increase in sensitivity is compensated in part by the smaller volume of a 1.3 mm rotor (4 µL in comparison to 20 µL). However, more efficient sedimentation at higher rotation frequencies induces a more than proportional increase in sensitivity (see below). Taken together, we expect a sensitivity of 10-30:1 in a $^{1}H,^{15}N$ correlation experiment for a 50S particle within 12 h. This is in fact observed experimentally (Figure 3)

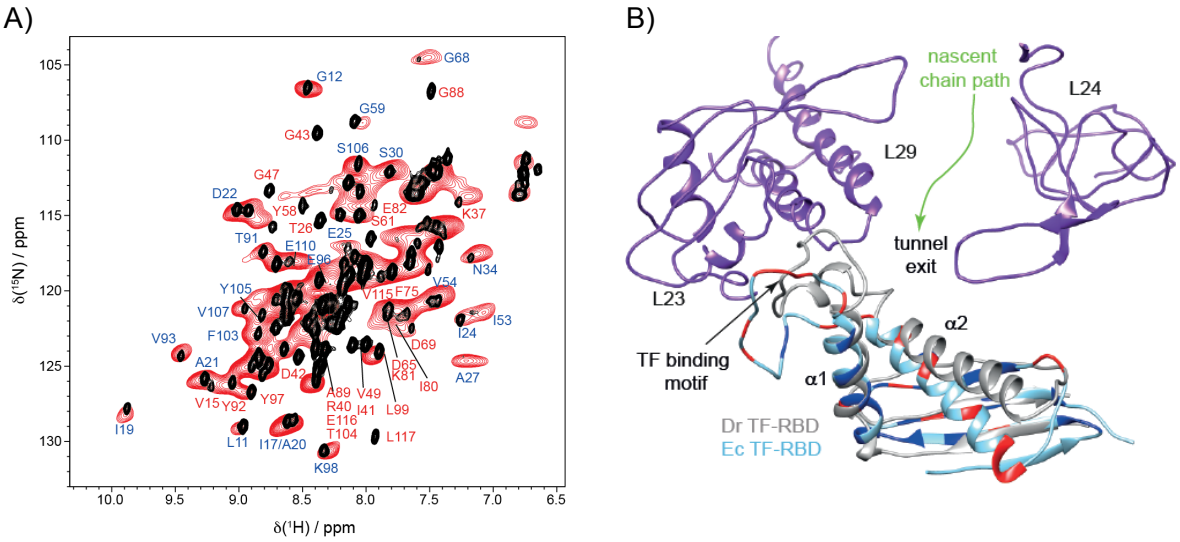

Figure 3: A) Superposition of a 2D solid-state ^{15}N-^{1}H correlation spectrum of *E.coli* [U-$^{1}H^{N}$,^{2}H,^{13}C,^{15}N]-labeled TF-RBD in complex with the *E.coli* 50S large ribosomal subunit (red) and a 2D solution-state ^{15}N-^{1}H correlation spectrum of free monomeric [U-$^{1}H^{N}$,^{2}H,^{13}C,^{15}N]-labeled TF-RBD (black). The solid-state NMR spectrum was recorded using a 850 MHz spectrometer, setting the MAS rotation frequency to 60 kHz. The solution-state reference spectrum was recoded on a 500 MHz spectrometer. In the annotation, blue color indicates residues for which chemical shifts do not change due to binding of TF-RBD to the ribosomes, and red color is employed to highlight resonances for which the peak either shifts or broadens beyond detection. B) Mapping of the NMR spectral changes onto the structure of TF-RBD. Alignment of the crystal structures of *D. radiodurans* TF-RBD in complex with the 50S ribosomal subunit (grey; pdb: 2d3o) with that of *E.coli* TF-RBD (light blue; pdb: 1w26). The ribosomal proteins L23, L29 and L24 at the tunnel exit and close to the binding site are shown in purple. The residues for which resonances are not affected by ribosome binding are shown in blue, those that exhibit chemical shift changes are shown in red, and those that could not be assigned due to spectral overlap are shown in grey. Reproduced with permission of Wiley from Barbet-Massin et al. [49].

Sedimentation fails to explain the intensities of differentially sized proteasome complexes

The proteasome is an essential cellular machinery, which is responsible for protein degradation, and thus for cellular protein homeostasis and viability [50]. The 20S proteasome of *Thermoplasma acidophilum* is ideally suited to demonstrate the FROSTY concept because of its modular assembly. The α-subunit (26 kDa) alone forms a double heptameric ring structure $\alpha_7\alpha_7$ (360 kDa) in solution. The native full proteasome core particle $\alpha_7\beta_7\beta_7\alpha_7$ (670 kDa) assembles upon addition of the β-subunit into a four ring barrel-like structure [51,

52]. The 1.1 MDa $11S_{14}$-$\alpha_7\beta_7\beta_7\alpha_7$ complex is formed through interaction with two heptameric 11S activator lids from *Trypanosoma brucei* on both sides of the $\alpha_7\beta_7\beta_7\alpha_7$ barrel. In the NMR experiments [10], only the α-subunit was isotopically enriched with ^{13}C and ^{15}N. All components of the protein complex were perdeuterated. Exchangeable sites were protonated using a ^{1}H:^{2}H mixing ratio of 1:4. The molecular weight of the respective proteasome assembly was successively increased by adding the NMR-invisible β-subunit and 11S activator. Figure 4 shows ^{15}N-filtered 1D spectra acquired for different 20S proteasome complexes from *Thermoplasma acidophilum*. Interestingly, the intensity of the respective spectra increases by more than a factor of 7 when the molecular weight of the complex is increased from 0.36 MDa to 1.1 MDa. Following Mainz et al. [10] and according to the theoretical work by Bertini et al. [8, 17], the fraction *f* of sedimented protein under MAS can be estimated as

$$f = \frac{c_{limit}\left(r^2 - a^2\right)}{c_0 r^2}$$

where

$$c_{limit} = \frac{0.74\,\rho_{prot}}{M_w}$$

and

$$a = \left(r^2 \left(1 - \frac{c_0}{c_{limit}} \right) + \left(\frac{2RT}{M_w \omega_r^2 \left(1 - \frac{\rho_{solv}}{\rho_{prot}} \right)} \right) \right)^{1/2}$$

In the equation, *r* refers to the inner radius of the rotor (i.e. 1.2 mm for a 3.2 mm MAS rotor). c_0 represents the initially employed protein oligomer concentration. Experimentally, we employed a concentration of $0.24*10^{-3}$ mol L^{-1} ($\alpha_7\alpha_7$), $0.14*10^{-3}$ mol L^{-1} ($\alpha_7\beta_7\beta_7\alpha_7$) and $0.21*10^{-3}$ mol L^{-1} ($11S_{14}$-$\alpha_7\beta_7\beta_7\alpha_7$), respectively. c_{limit} refers to the maximum protein concentration in the sediment calculated from the protein density ρ_{prot} (1,430 kg m^{-3}) and the molecular weight M_w of the protein complex (360 kDa for $\alpha_7\alpha_7$, 670 kDa for $\alpha_7\beta_7\beta_7\alpha_7$ and 1.1 MDa for $11S_{14}$-$\alpha_7\beta_7\beta_7\alpha_7$). Assuming a packing coefficient of 0.74 for spherical particles, the maximum oligomer concentration c_{limit} can thus be estimated as $2.91*10^{-3}$ mol L^{-1} ($\alpha_7\alpha_7$), $1.58*10^{-3}$ mol L^{-1} ($\alpha_7\beta_7\beta_7\alpha_7$) and $1.04*10^{-3}$ mol L^{-1} ($11S_{14}$-$\alpha_7\beta_7\beta_7\alpha_7$), respectively. The parameter *a* corresponds to the distance from the rotor axis at which the maximum protein concentration c_{limit} is reached. ω_r denotes the MAS rotation frequency (22 kHz), ρ_{solv} the density of the solvent (1,085 kg·m^{-3} for a 30% glycerol/water mixture at 273 K), *T* the temperature (273 K) and *R* the universal gas constant (8.314 J mol^{-1} K^{-1}). Using these values, the fraction *f* of MAS-sedimented protein can be estimated to be on the order of 97.7 % ($\alpha_7\alpha_7$), 98.8 % ($\alpha_7\beta_7\beta_7\alpha_7$) and 99.7 % ($11S_{14}$-$\alpha_7\beta_7\beta_7\alpha_7$), respectively. These calculations contradict the observed differences in signal intensities and indicate that there is still residual mobility in the sediment, which presumably induces exchange broadening.

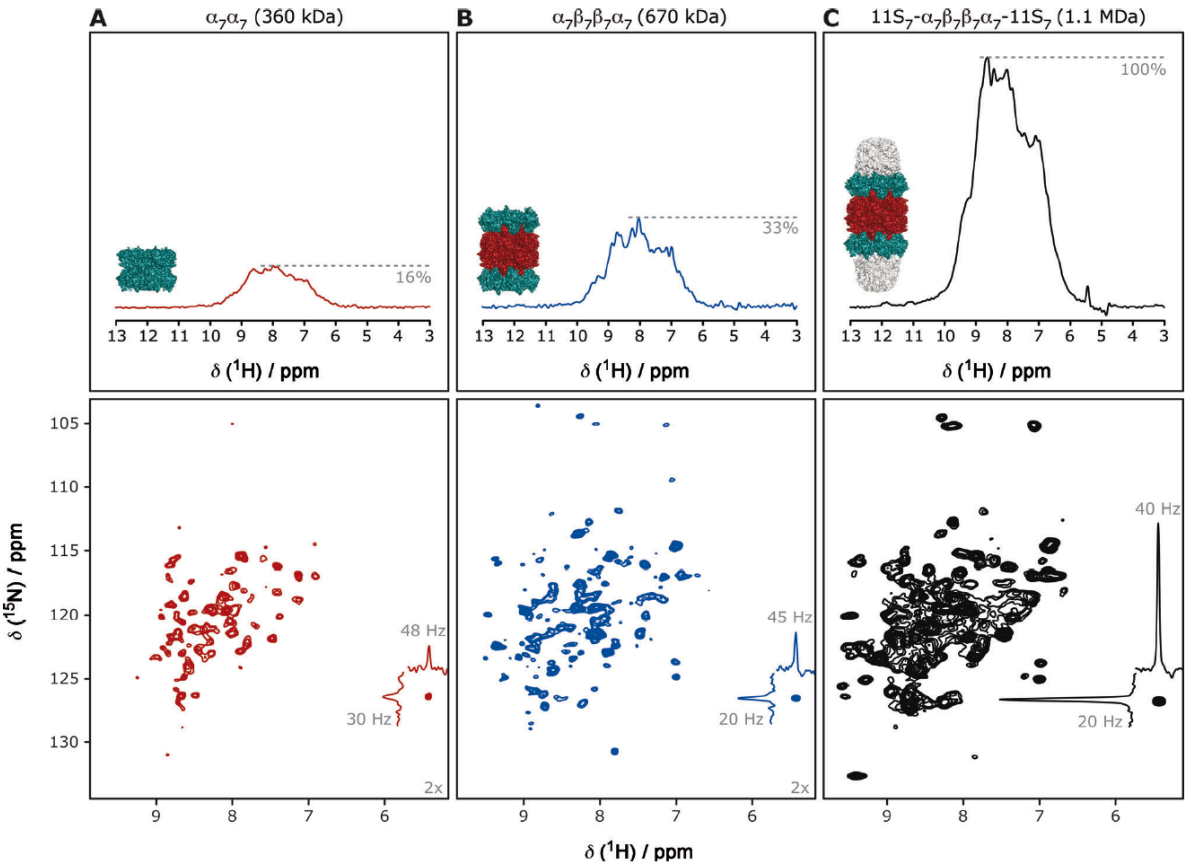

Figure 4. Proton-detected MAS experiments and the effect of increasing molecular weight for different assemblies of the 20S proteasome of *Thermoplasma acidophilum*. CP-based 2D ^{1}H-^{15}N correlation spectra are shown on the bottom, the corresponding 1D versions are represented on the top for the 360 kDa $\alpha_7\alpha_7$ *(A)*, the 670 kDa $\alpha_7\beta_7\beta_7\alpha_7$ *(B)* and the 1.1 MDa 11S-$\alpha_7\beta_7\beta_7\alpha_7$-11S complex *(C)*. The spectra were recorded at 0 °C and with 22 kHz MAS. Acquisition and processing parameters were identical. The signal intensities of ^{15}N-filtered ^{1}H-1D spectra are normalized to account for the different concentrations of the α-subunit. The calculated fraction of sedimented protein amounts to 97.7%, 98.8% and 99.7% for $\alpha_7\alpha_7$, $\alpha_7\beta_7\beta_7\alpha_7$ and 11S-$\alpha_7\beta_7\beta_7\alpha_7$-11S, respectively. Figure reproduced with permission from Wiley [10].

Molecular crowding impacts both translational and rotational diffusion of a protein. Whereas translational diffusion is largely determined by viscosity, intermolecular protein-protein interactions have a much smaller effect on rotational diffusion [53]. At very high concentrations globular proteins typically retain a high degree of rotational mobility as they can rotate rather freely within a cage. It is found that the correlation time of rotational diffusion τ_R is proportional to the molecular weight M_W following the relation τ_R (µs) ~ $M_W^{3/d}$ (kDa), with d being approximately d=2.5 [53]. Depending on temperature, a rotational correlation time τ_R on the order of 1.2-5.7 µs was found for αB-crystallin [9, 53]. An increase in the protein concentration from 35 mg/mL to 180 mg/mL results in an increase of rotational diffusion by a factor of approximately 1.5 [53]. The protein concentration in a sediment is approximately $\rho_{prot} \cdot 0.74$ = 1050 mg/mL. This concentration is obviously much higher than what is accessible with an analytical technique. Rotational diffusion might increase more than linear in this concentration regime.

High Viscosity Solutions yield CP transfers

Ionic liquids (IL) and Deep Eutectic Solvents (DES) are obtained by mixing certain solid chemicals in a defined molar ratio [54, 55]. IL and DES play an important role for biological function in living cells. They allow to solubilize and transport metabolites that are not soluble in water. Biological DES are called Natural Deep Eutectic Solvents (NADES) [56, 57]. NADES are characterized by very high viscosities and low melting temperatures. For several NADES, intermolecular NOEs have been observed between solvent molecules, suggesting intermolecular hydrogen bonding [57]. NADES show glass transition temperatures of around –50°C without having a melting point. They form a stable liquid over a wide range of temperatures, indicating that NADES might play an important role in plants for cold resistance. We employed the NADES GCh (a mixture of glucose, choline chloride and water in a molar ratio of 1:1:4) to carry out the experiments described below. To prepare the sample, the solid chemicals (glucose and choline chloride) were mixed first in the respective molar ratio in an extra dry beaker. Subsequently, water was added to this mixture, which was heated up to 70°C under constant stirring for about 20 hours until all material was dissolved. The temperature was then lowered to room temperature to obtain a clear and transparent solution. Subsequently, the highly viscous solution was transferred into a 3.2 mm MAS rotor. In the NMR experiment, we found that proton polarization can be transferred to the glucose carbons using cross-polarization. CP transfer works particularly well at low temperatures and low (3 kHz) MAS frequencies (Figure 5A). Under these conditions, GCh cannot sediment on the wall of the rotor. The CP transfer efficiency increases with a decrease in temperature. The viscosity of this NADES is strongly temperature dependent and changes from 349 cP at 23°C to 2569 cP at -3°C, and 5019 cP at -10°C. These experiments suggest that CP might be due to a rotational immobilization of the solvent molecules due to their high viscosity. To estimate the fraction of the sample that behaves solid-like, we analyzed the intensity ratio obtained from $^{1}H,^{13}C$ CP and ^{13}C direct excitation experiments. As expected, the CP intensity of the GCh sample increases as the temperature decreases. At a temperature of 250 K, 14 % of the GCh sample behaves solid-like (normalizing the CP transfer efficiency to 100 %). Figure 5B represents the relative CP versus direct ^{13}C signal intensity (I^{CP}/I^{direct}) as a function of the MAS rotation frequency. We observe a slight increase of the CP signal at slower frequencies, indicating that CP transfer is not originating from a sedimentation induced immobilization.

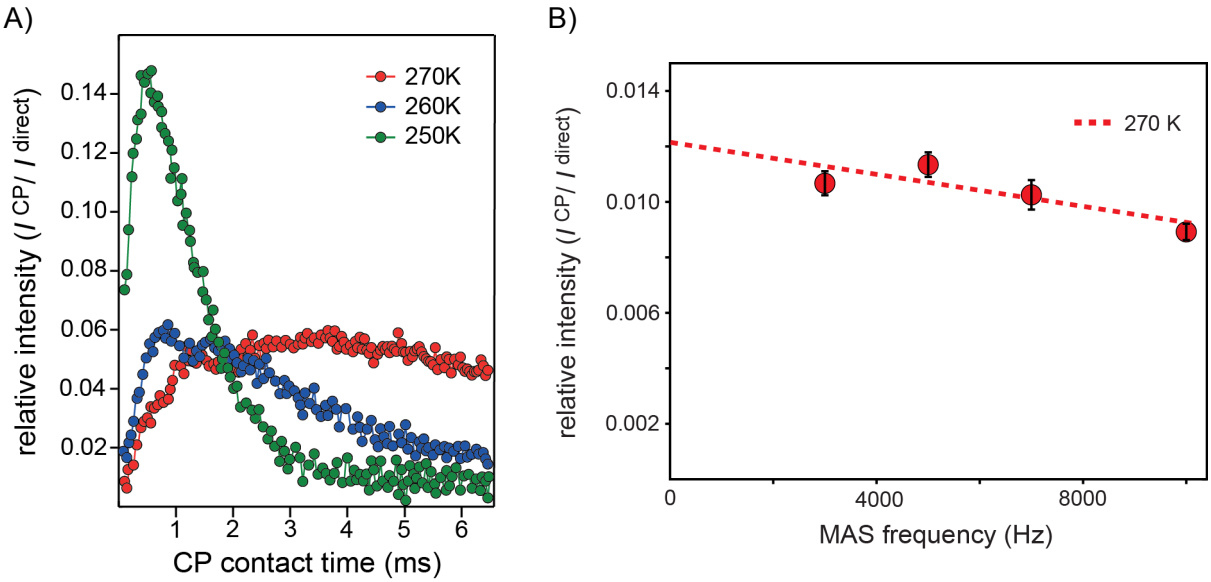

Figure 5. A) $^{1}H,^{13}C$ CP build up for the NADES GCh (glucose : choline chloride : water = 1:1:4) as a function of temperature (red: 270 K, blue: 260 K and green: 250 K). Experiments were carried out at 9.4 T (corresponding to a ^{1}H Larmor frequency of 400 MHz) and a MAS frequency of 3 kHz. The y-axis represents the relative intensity obtained in a CP experiment in comparison to the intensity that was measured in a direct ^{13}C excitation experiment. **B)** Relative CP versus direct signal intensity as a function of the MAS rotation frequency for different sample temperatures. Care was taken to correct the actual sample temperature with respect to sample spinning. The sample employed to record the MAS frequency dependence is distinct to the sample that was used to record the MAS buildup curve represented in A). Deviations are due to slightly different sample conditions.

CONCLUSION

Taken together, we have shown how solutions of high molecular weight protein complexes can be studied using MAS solid-state NMR methodology. The approach is ideally suited to study heterogeneous systems such as weakly interacting chaperone-amyloid complexes that are not suitable for crystallography and have too high molecular weight for traditional solution-state NMR approaches. Titration experiments that are routinely performed in solution-state NMR can now also be envisaged for "solid-state" NMR applications. We expect that smaller diameter rotors that allow to achieve higher MAS rotation frequencies and a larger centrifugal acceleration in combination with proton detection allow the investigation of even smaller amounts of sample with high sensitivity. It will be interesting to see how the remaining discrepancies in the explanation of the FROSTY/sedNMR approach can be reconciled in the future.

ACKNOWLEDGEMENT

This work was performed in the framework of the SFB-1035/Project-B07 (German Research Foundation, DFG). This research was supported by the Helmholtz-Gemeinschaft, and the DFG (Re1435). We are grateful to the Center for Integrated Protein Science Munich (CIPS-M) for financial support.

REFERENCES

[1] A.K. Paravastu, R.D. Leapman, W.-M. Yau, R. Tycko, Molecular structural basis for polymorphism in Alzheimer's beta-amyloid fibrils, Proc. Natl Acad. Sci. U.S.A., 105 (2008) 18349-18354.

[2] A.K. Schutz, T. Vagt, M. Huber, O.Y. Ovchinnikova, R. Cadalbert, J. Wall, P. Guntert, A. Bockmann, R. Glockshuber, B.H. Meier, Atomic-Resolution Three-Dimensional Structure of Amyloid beta Fibrils Bearing the Osaka Mutation, Angewandte Chemie Int. Edt. Engl., 54 (2015) 331-335.

[3] S.A. Shahid, B. Bardiaux, W.T. Franks, L. Krabben, M. Habeck, B.-J. van Rossum, D. Linke, Membrane-protein structure determination by solid-state NMR spectroscopy of microcrystals, Nature Methods, 9 (2012) 1212-U1119.

[4] L.B. Andreas, M. Reese, M.T. Eddy, V. Gelev, Q.Z. Ni, E.A. Miller, L. Emsley, G. Pintacuda, J.J. Chou, R.G. Griffin, Structure and Mechanism of the Influenza A M2(18-60) Dimer of Dimers, J. Am. Chem. Soc., 137 (2015) 14877–14886.

[5] E.R. Andrew, A. Bradbury, R.G. Eades, NMR Spectra Recorded from a Crystal Rotated at High Speed, Nature, 182 (1958) 1659-1659.

[6*] A. Mainz, S. Jehle, B.J. van Rossum, H. Oschkinat, B. Reif, Large Protein Complexes with Extreme Rotational Correlation Times Investigated in Solution by Magic-Angle-Spinning NMR Spectroscopy, J. Am. Chem. Soc., 131 (2009) 15968–15969.
(First practical implementation of the FROSTY/SedNMR approach).

[7] A. Mainz, B. Bardiaux, F. Kuppler, G. Multhaup, I.C. Felli, R. Pierattelli, B. Reif, Structural and mechanistic implications of metal-binding in the small heat-shock protein αB-crystallin, J. Biol. Chem., 287 (2012) 1128-1138.

[8*] I. Bertini, C. Luchinat, G. Parigi, E. Ravera, B. Reif, P. Turano, Solid-state NMR of proteins sedimented by ultracentrifugation, Proc. Natl Acad. Sci. U.S.A., 108 (2011) 10396-10399.
(first paper to suggest that sedimentation induces an immobilization of the molecules of the sample)

[9] E. Ravera, G. Parigi, A. Mainz, T.L. Religa, B. Reif, C. Luchinat, Experimental determination of microsecond reorientation correlation times in protein solutions, J. Phys. Chem. B, 117 (2013) 3548-3553.

[10*] A. Mainz, T. Religa, R. Sprangers, R. Linser, L.E. Kay, B. Reif, NMR Spectroscopy of Soluble Protein Complexes at One Mega-Dalton and Beyond, Angewandte Chemie Int. Edt. Engl., 52 (2013) 8746–8751.
(First backbone assignment of a MDa protein complex in solution).

[11] C. Gardiennet, A.K. Schutz, A. Hunkeler, B. Kunert, L. Terradot, A. Bockmann, B.H. Meier, A Sedimented Sample of a 59 kDa Dodecameric Helicase Yields High-Resolution Solid-State NMR Spectra, Angewandt. Chem. Int. Edt., 51 (2012) 7855-7858.

[12] J. Horwitz, Alpha crystallin: The quest for a homogeneous quaternary structure, Exp. Eye Res., 88 (2009) 190-194.

[13] J.A. Aquilina, J.L.P. Benesch, O.A. Bateman, C. Slingsby, C.V. Robinson, Polydispersity of a mammalian chaperone: Mass spectrometry reveals the population

of oligomers in alpha B-crystallin, Proc. Natl Acad. Sci. U.S.A., 100 (2003) 10611-10616.
[14] M.F. Ahmad, D. Singh, A. Taiyab, T. Ramakrishna, B. Raman, C.M. Rao, Selective Cu2+ Binding, Redox Silencing, and Cytoprotective Effects of the Small Heat Shock Proteins αA- and αB-Crystallin, J. Mol. Biol., 382 (2008) 812–824.
[15] M.L. Ganadu, Aru, M., Mura, G.M., Coi, A., Mlynarz, P., Kozlowski, H., Effects of divalent metal ions on the alphaB-crystallin chaperone-like activity: spectroscopic evidence for a complex between copper(II) and protein, J. Inorg. Biochem., 98 (2004) 1103-1109.
[16] I. Bertini, G. Gallo, M. Korsak, C. Luchinat, J. Mao, E. Ravera, Formation kinetics and structural features of Beta-amyloid aggregates by sedimented solute NMR, Chembiochem, 14 (2013) 1891-1897.
[17] I. Bertini, C. Luchinat, G. Parigi, E. Ravera, SedNMR: On the Edge between Solution and Solid-State NMR, Acc. Chem. Res., 46 (2013) 2059-2069.
[18] G.S. Hisao, M.A. Harland, R.A. Brown, D.A. Berthold, T.E. Wilson, C.M. Rienstra, An efficient method and device for transfer of semisolid materials into solid-state NMR spectroscopy rotors, J. Magn. Reson., in press (2016).
[19] E. Ravera, B. Corzilius, V.K. Michaelis, C. Luchinat, R.G. Griffin, I. Bertini, DNP-Enhanced MAS NMR of Bovine Serum Albumin Sediments and Solutions, J. Phys. Chem. B, 118 (2014) 2957-2965.
[20] Y. Ding, L.M. Fujimoto, Y. Yao, F.M. Marassi, Solid-state NMR of the Yersinia pestis outer membrane protein Ail in lipid bilayer nanodiscs sedimented by ultracentrifugation, J. Biomol. NMR, 61 (2015) 275-286.
[21] F. Hagn, M. Etzkorn, T. Raschle, G. Wagner, Optimized Phospholipid Bilayer Nanodiscs Facilitate High-Resolution Structure Determination of Membrane Proteins, J. Am. Chem. Soc., 135 (2013) 1919-1925.
[22] A. Mainz, J. Peschek, M. Stavropoulou, K. Back, B. Bardiaux, S. Asami, E. Prade, C. Peters, S. Weinkauf, J. Buchner, B. Reif, The Chaperone αB--Crystallin Deploys Different Interfaces to Capture an Amorphous and an Amyloid Client, Nature Struct. Mol. Biol., 22 (2015) 898-905.
[23] S. Jehle, P. Rajagopal, B. Bardiaux, S. Markovic, R. Kuhne, J.R. Stout, V.A. Higman, R.E. Klevit, B.-J. van Rossum, H. Oschkinat, Solid-state NMR and SAXS studies provide a structural basis for the activation of alpha B-crystallin oligomers, Nature Struct. Mol. Biol., 17 (2010) 1037-1043.
[24] A. Laganowsky, J.L.P. Benesch, M. Landau, L. Ding, M.R. Sawaya, D. Cascio, Q. Huang, C.V. Robinson, J. Horwitz, D. Eisenberg, Crystal structures of truncated alphaA and alphaB crystallins reveal structural mechanisms of polydispersity important for eye lens function, Protein Science, 19 (2010) 1031-1043.
[25] S.P. Delbecq, S. Jehle, R. Klevit, Binding determinants of the small heat shock protein, alpha B-crystallin: recognition of the 'IxI' motif, Embo Journal, 31 (2012) 4587-4594.
[26] A.J. Baldwin, G.R. Hilton, H. Lioe, C. Bagneris, J.L.P. Benesch, L.E. Kay, Quaternary Dynamics of alpha B-Crystallin as a Direct Consequence of Localised Tertiary Fluctuations in the C-Terminus, J. Mol. Biol., 413 (2011) 310-320.
[27] S. Jehle, B.-J. van Rossum, J.R. Stout, S.M. Noguchi, K. Falber, K. Rehbein, H. Oschkinat, R.E. Klevit, P. Rajagopal, alpha B-Crystallin: A Hybrid Solid-State/Solution-State NMR Investigation Reveals Structural Aspects of the Heterogeneous Oligomer, J. Mol. Biol., 385 (2009) 1481-1497.
[28] S. Jehle, B.S. Vollmar, B. Bardiaux, K.K. Dove, P. Rajagopal, T. Gonen, H. Oschkinat, R.E. Klevit, N-terminal domain of αB-crystallin provides a conformational switch for multimerization and structural heterogeneity, Proc. Natl Acad. Sci. U.S.A., 108 (2011) 6409-6414.
[29] N. Braun, M. Zacharias, J. Peschek, A. Kastenmuller, J. Zou, M. Hanzlik, M. Haslbeck, J. Rappsilber, J. Buchner, S. Weinkauf, Multiple molecular architectures of the eye

lens chaperone alpha B-crystallin elucidated by a triple hybrid approach, Proc. Natl Acad. Sci. U.S.A., 108 (2011) 20491-20496.
[30] V. Chevelkov, K. Rehbein, A. Diehl, B. Reif, Ultra-high resolution in proton solid-state NMR at high levels of deuteration, Angew. Chem. Int. Ed., 45 (2006) 3878-3881.
[31] Ü. Akbey, S. Lange, T.W. Franks, R. Linser, A. Diehl, B.J. van Rossum, B. Reif, H. Oschkinat, Optimum Levels of Exchangeable Protons in Perdeuterated Proteins for Proton Detection in MAS Solid-State NMR Spectroscopy, J. Biomol. NMR 46 (2010) 67–73.
[32] V. Agarwal, A. Diehl, N. Skrynnikov, B. Reif, High Resolution ^{1}H Detected ^{1}H,^{13}C Correlation Spectra in MAS Solid-State NMR using Deuterated Proteins with Selective ^{1}H,^{2}H Isotopic Labeling of Methyl Groups, J. Am. Chem. Soc., 128 (2006) 12620-12621.
[33] V. Agarwal, Y. Xue, B. Reif, N.R. Skrynnikov, Protein side-chain dynamics as observed by solution- and solid-state NMR: a similarity revealed, J. Am. Chem. Soc., 130 (2008) 16611–16621.
[34] V. Agarwal, B. Reif, Residual Methyl Protonation in Perdeuterated Proteins for Multidimensional Correlation Experiments in MAS solid-state NMR Spectroscopy, J. Magn. Reson., 194 (2008) 16-24.
[35] S. Asami, P. Schmieder, B. Reif, High resolution 1H-detected solid-state NMR spectroscopy of protein aliphatic resonances: Access to tertiary structure information, J. Am. Chem. Soc., 132 (2010) 15133–15135.
[36] S. Asami, B. Reif, Proton-detected solid-state NMR at aliphatic sites: Applications to Crystalline Systems, Acc. Chem. Res., 46 (2013) 2089-2097.
[37] S. Asami, J.R. Porter, O.F. Lange, B. Reif, Access to Cα backbone dynamics of biological solids by (13)C-T1 relaxation and molecular dynamics simulation, J. Am. Chem. Soc., 137 (2015) 1094-1100.
[38] T. Sinnige, M. Daniels, M. Baldus, M. Weingarth, Proton Clouds to Measure Long-Range Contacts between Nonexchangeable Side Chain Protons in Solid-State NMR, J. Am. Chem. Soc., 136 (2014) 4452-4455.
[39] J.R. Lewandowski, J.N. Dumez, U. Akbey, S. Lange, L. Emsley, H. Oschkinat, Enhanced Resolution and Coherence Lifetimes in the Solid-State NMR Spectroscopy of Perdeuterated Proteins under Ultrafast Magic-Angle Spinning, J. Phys. Chem. Lett., 2 (2011) 2205-2211.
[40] R. Linser, M. Dasari, M. Hiller, V. Higman, U. Fink, J.-M. Lopez del Amo, L. Handel, B. Kessler, P. Schmieder, D. Oesterhelt, H. Oschkinat, B. Reif, Proton detected solid-state NMR of fibrillar and membrane proteins, Angew. Chem. Int. Ed., 50 (2011) 4508-4512.
[41] V.K. Morris, R. Linser, K.L. Wilde, A.P. Duff, M. Sunde, A.H. Kwan, Solid-State NMR Spectroscopy of Functional Amyloid from a Fungal Hydrophobin: A Well-Ordered beta-Sheet Core Amidst Structural Heterogeneity, Angewandt. Chem. Int. Edt., 51 (2012) 12621-12625.
[42] V. Agarwal, R. Linser, M. Dasari, U. Fink, J.-M. Lopez del Amo, B. Reif, Hydrogen bonding involving side chain exchangeable groups stabilizes amyloid quarternary structure, Phys. Chem. Chem. Phys., 15 (2013) 12551 - 12557.
[43] M.E. Ward, L. Shi, E. Lake, S. Krishnamurthy, H. Hutchins, L.S. Brown, V. Ladizhansky, Proton-Detected Solid-State NMR Reveals Intramembrane Polar Networks in a Seven-Helical Transmembrane Protein Proteorhodopsin, J. Am. Chem. Soc., 133 (2011) 17434-17443.
[44] E. Barbet-Massin, M. Felletti, R. Schneider, S. Jehle, G. Communie, N. Martinez, M.R. Jensen, R.W.H. Ruigrok, L. Emsley, A. Lesage, M. Blackledge, G. Pintacuda, Insights into the Structure and Dynamics of Measles Virus Nucleocapsids by H-1-detected Solid-state NMR, Biophys. J., 107 (2014) 941-946.

[45] V. Chevelkov, B. Habenstein, A. Loquet, K. Giller, S. Becker, A. Lange, Proton-detected MAS NMR experiments based on dipolar transfers for backbone assignment of highly deuterated proteins, J. Magn. Reson., 242 (2014) 180-188.
[46] V. Agarwal, S. Penzel, K. Szekely, R. Cadalbert, E. Testori, A. Oss, J. Past, A. Samoson, M. Ernst, A. Bockmann, B.H. Meier, De Novo 3D Structure Determination from Sub-milligram Protein Samples by Solid-State 100 kHz MAS NMR Spectroscopy, Angewandt. Chem. Int. Edt., 53 (2014) 12253-12256.
[47] J.M. Lamley, D. Iuga, C. Oster, H.J. Sass, M. Rogowski, A. Oss, J. Past, A. Reinhold, S. Grzesiek, A. Samoson, J.R. Lewandowski, Solid-State NMR of a Protein in a Precipitated Complex with a FullLength Antibody, J. Am. Chem. Soc., 136 (2014) 16800-16806.
[48] A. Bockmann, M. Ernst, B.H. Meier, Spinning proteins, the faster, the better?, J. Magn. Reson., 253 (2015) 71-79.
[49*] E. Barbet-Massin, C.-T. Huang, V. Daebel, S.-T.D. Hsu, B. Reif, Site-Specific Solid-State NMR Studies of “Trigger Factor” in Complex with the Large Ribosomal Subunit 50S, Angewandte Chemie Int. Edt. Engl., 54 (2015) 4367–4369.
(First backbone correlation experiments for an asymmetric MDa protein complex).
[50] W. Baumeister, J. Walz, F. Zuhl, E. Seemuller, The proteasome: Paradigm of a self-compartmentalizing protease, Cell, 92 (1998) 367-380.
[51] J. Lowe, D. Stock, R. Jap, P. Zwickl, W. Baumeister, R. Huber, Crystal Structure of the 20S Proteasome from the Archaeon T.acidophilum at 3.4 Angstrom Resolution, Science, 268 (1995) 533-539.
[52] A. Forster, E.I. Masters, F.G. Whitby, H. Robinson, C.P. Hill, The 1.9 A structure of a proteasome-11S activator complex and implications for proteasome-PAN/PA700 interactions, Mol. Cell, 18 (2005) 589-599.
[53] M. Roos, S. Link, J. Balbach, A. Krushelnitsky, K. Saalwachter, NMR-Detected Brownian Dynamics of alpha B-Crystallin over a Wide Range of Concentrations, Biophys. J., 108 (2015) 98-106.
[54] R.D. Rogers, K.R. Seddon, Ionic liquids - Solvents of the future?, Science, 302 (2003) 792-793.
[55] A.P. Abbott, D. Boothby, G. Capper, D.L. Davies, R.K. Rasheed, Deep eutectic solvents formed between choline chloride and carboxylic acids: Versatile alternatives to ionic liquids, J. Am. Chem. Soc., 126 (2004) 9142-9147.
[56] Y.T. Dai, J. van Spronsen, G.J. Witkamp, R. Verpoorte, Y.H. Choi, Natural deep eutectic solvents as new potential media for green technology, Anal. Chimica Acta, 766 (2013) 61-68.
[57] Y.T. Dai, G.J. Witkamp, R. Verpoorte, Y.H. Choi, Tailoring properties of natural deep eutectic solvents with water to facilitate their applications, Food Chem., 187 (2015) 14-19.